



OPEN ACCESS

EDITED BY

Yanjin Lu,
Chinese Academy of Sciences (CAS),
China

REVIEWED BY

Qiang Wang,
China Medical University, China
Jinxin Lin,
Fujian Normal University, China

*CORRESPONDENCE

Xiaofeng Huang,
✉ xiaofengh@ccmu.edu.cn

RECEIVED 27 April 2023

ACCEPTED 13 June 2023

PUBLISHED 13 July 2023

CITATION

Li Y, Tang L, Shen M, Wang Z and Huang X (2023), A comparative study of Sr-loaded nano-textured Ti and TiO₂ nanotube implants on osseointegration immediately after tooth extraction in Beagle dogs.
Front. Mater. 10:1213163.
doi: 10.3389/fmats.2023.1213163

COPYRIGHT

© 2023 Li, Tang, Shen, Wang and Huang. This is an open-access article distributed under the terms of the [Creative Commons Attribution License \(CC BY\)](https://creativecommons.org/licenses/by/4.0/). The use, distribution or reproduction in other forums is permitted, provided the original author(s) and the copyright owner(s) are credited and that the original publication in this journal is cited, in accordance with accepted academic practice. No use, distribution or reproduction is permitted which does not comply with these terms.

A comparative study of Sr-loaded nano-textured Ti and TiO₂ nanotube implants on osseointegration immediately after tooth extraction in Beagle dogs

Yongfeng Li¹, Li Tang², Mingming Shen¹, Zhen Wang¹ and Xiaofeng Huang^{1*}

¹Department of Stomatology, Beijing Friendship Hospital, Capital Medical University, Beijing, China, ²School of Stomatology, Qingdao University, Qingdao, China

Dental implantation, when performed immediately after tooth extraction, simplifies the treatment procedure, resulting in satisfaction for dentists and patients. Dental implants with nanotopography surface modification have been used to promote osseointegration immediately after implantation. We compared two different nanotopography surface implants on the effects of osseointegration immediately after tooth extraction: TiO₂ nanotubes (NT-TiO₂) fabricated by anodization and Sr-loaded nanotopography Ti (NT-Sr) formed via magnetron sputtering technology. Sr-loaded nanotextured Ti nanotubes (NT-Sr) were fabricated via magnetron sputtering using 99.99% SrTiO₃ as the sputtering target. TiO₂ nanotubes (NT-TiO₂) were fabricated by anodization in 0.5 wt% hydrofluoric acid (HF). After the surface topography, hydrophilicity, chemical components, and interface bonding strength were analyzed, two different nano-topographies were applied for *in vivo* cellular activity evaluation. Subsequently, the implants with NT-Sr and NT-TiO₂ surfaces were inserted into the fresh socket immediately after tooth extraction. Radiological scanning, histological analysis, and biomechanical tests were carried out to investigate implant osseointegration. The results showed that nanotubes with diameters of 15–80 nm were distributed on the NT-TiO₂ surface, while the NT-Sr group showed 20–40 nm nanoparticles deposited on the surface. Compared to NT-Sr, the NT-TiO₂ surface possessed better hydrophilicity and favorable cellular adhesion and proliferation. The NT-Sr surface possessed greater interfacial bonding strength than the NT-TiO₂ group, and greater bone formation, higher bone-to-implant contact (BIC%), and maximum pull-out force were observed in the NT-Sr group. The above results indicated that although the NT-TiO₂ surface showed favorable *in vitro* bioactivity, the NT-Sr surface, with higher interface bonding strength, showed better *in vitro* osteogenesis, and would be more favorable for immediate implantation.

KEYWORDS

strontium, nano, magnetron sputtering, osseointegration, surface modification, immediate implantation

1 Introduction

Immediate implant placement after tooth extraction has led to much satisfaction for dentists and patients over the past decades (Seyssens et al., 2022). Compared to traditional delayed implantation, immediate implants can simplify the treatment procedure. In addition, immediate implantation is favorable for preservation of the extraction site and decreases alveolar bone resorption (Araújo et al., 2019). In order to attain comparable long-term clinical efficacy to delayed implantation, immediate implantation demands higher yields of early osteogenic ability around the implant and higher initial stability. Various strategies have been developed to achieve early osteogenesis and initial stability during immediate implantation, including implant thread optimization and implant surface roughening. Previous studies have demonstrated that rough implant surface modifications can induce osteogenesis around the implant and subsequently stabilize osseointegration (Robo et al., 2022). To date, the conventional topography of commercial implant is almost at the micro-scale (1–10 μm). At present, nano scale surface (1–100 nm) modification has received significant attention, owing to its favorable biological reaction compared to micro-scale surface implants (Mendonça et al., 2008; Cavalu et al., 2020).

Previous studies have reported that a nanotopography surface promotes the osseointegration of implants. Nanotopography structures are classified, according to their topography, as nanoparticles, nanotubes, nanofibers (Mendonça et al., 2008; Yeo, 2019), and so on. An *in vitro* study conducted by Long et al. reported that titanium dioxide (TiO_2) nanotubes can create a favorable osteoimmunomodulatory environment for bone regeneration and osseointegration (Bai et al., 2021). Parnia found that dental implants with nanoparticle coatings possess enhanced osseointegration and antimicrobial properties (Feridoun et al., 2017). Our previous studies have demonstrated that strontium (Sr)-loaded nanoparticle surfaces can promote osteogenesis in cellular and animal experiments under normal and osteoporotic conditions. However, surface roughness modification is a double-edged sword; an active roughness surface may decrease the coating interface bonding strength of the implant. Therefore, it is meaningful to fabricate surfaces possessing the dual properties of high coating interface bonding strength and active osteogenic ability. Few studies have investigated the effects of different nanotopographic surfaces on osseointegration in immediate implantation, especially when applied to large animal models.

Therefore, this study was performed to compare effects of two different typical nanotopographic surfaces on osseointegration during immediate implantation: Sr-loaded nanotextured Ti nanotubes (NT-Sr) and TiO_2 nanotubes (NT- TiO_2).

2 Materials and methods

2.1 Sample coating fabrication and investigation

Titanium disks (Φ 15 mm \times 1 mm) and titanium screw implants (Φ 4 mm \times 8 mm) were randomly divided into two groups. The NT- TiO_2 implant group was prepared via anodization

in a 0.5% (w/v) hydrofluoric (HF) acid electrolyte solution for 30 min, using a 20 V direct current (DC) power supply, and a platinum electrode as the cathode. NT-Sr group implants were fabricated via magnetron sputtering using an industrial physical vapor deposition (PVD) system. The films were deposited under the following conditions: Ar_2 gas composition at 0.5 Pa. After fabrication, all samples were cleaned sequentially with acetone, ethanol, and deionized water ultrasonically, and finally sterilized with γ irradiation for subsequent testing. The samples were tested using field-emission scanning electron microscopy (FE-SEM, HITACHI S-4800) to observe the surface topography and X-ray photoelectron spectroscopy (XPS, ESCALB MK-II) for chemical component analysis.

The interfacial bonding strength of nanotopography layers was evaluated using an epoxy resin docking tensile test, and the Ti samples after epoxy resin docking tensile testing were investigated using SEM to evaluate the collapsed surface characteristics. The surface hydrophilicity of the Ti samples was measured using a surface contact angle measurement machine (DSA30; Kruss, Germany).

The Sr release experiment was carried out using the following procedures: NT-Sr samples were immersed in 5 mL phosphate buffer solution (PBS, Gibco) at 37°C. The PBS was collected and replaced with fresh PBS after 1, 4, 7, and 14 days. The PBS solution containing released Sr was analyzed using inductively coupled plasma atomic emission spectrometry (ICP-AES; IRIS Advantage ER/S). The NT-Sr samples were completely dissolved in a HNO_3 and HF mixture with ultrasonic treatment at room temperature. The total amount of Sr was determined using ICP-AES.

2.2 *In vitro* cellular assay

The murine MC3T3-E1 osteoblast cell line was used for co-culture with Ti samples. The cells were cultured in a minimum essential medium (α -MEM, Gibco) containing 10% fetal calf serum (FCS, Gibco) at 37°C, with the medium changed every 3 days. The Ti samples were placed in a 24-well plate and the cells were seeded at a density of 2×10^4 cells/mL for the assays.

Cell adhesion analysis was carried out after incubation for 30, 60, and 120 min; the attached cells were stained using 4',6'-diamidino-2-phenylindole (DAPI) (Sigma-Aldrich Co., St Louis, MO, United States). Positive cells were counted under an optical microscope (Olympus FluoView FV1000).

Cell proliferation was assessed after culturing for 1, 4, and 7 days using a 3-(4,5-dimethylthiazol-2-yl)-2, 5-diphenyltetrazolium bromide (MTT) (Sigma-Aldrich Co.) assay. At prescribed time points, the Ti samples were gently rinsed with PBS and transferred to a new plate. The Ti samples were then incubated with the MTT solution at 37°C for 4 h. The formazan was then dissolved in dimethyl sulfoxide, and the optical density was measured at 490 nm using a spectrophotometer (Bio-Tek).

Alkaline phosphatase activity (ALP) analysis was performed after 7 days in culture. A colorimetric assay was used to determine the quantity of ALP present. This assay was based on an ALP reagent containing p-nitrophenyl phosphate (p-NPP) as the substrate. Moreover, cell morphology observation after incubation for 3 days was carried out to compare the *in vitro* cellular activity of the two nano-texture surfaces. After incubation for 3 days, the samples with

attached cells were fixed in 3% glutaraldehyde, dehydrated in a graded ethanol series, freeze dried, sputter coated with gold, and observed using FE-SEM. The details of the above *in vitro* cellular assay complied with our previous study (Li et al., 2015).

2.3 *In vivo* experiment

2.3.1 Animals and surgical procedures

Eight 2-year-old beagles were included in our study. The study was approved and supervised by the Laboratory Animal Ethical Inspection, School of the Fourth Military Medical University [Xi'an, China; approval document no. 2014 (058)]. Adequate measures were taken to minimize pain and discomfort in animals. Animals were anesthetized with sodium pentobarbital (30 mg/kg; Merck Drugs and Biotechnology). The two different surface implants were inserted into fresh extraction sockets immediately after bilateral mandibular premolar extraction. The NT-TiO₂ implants were implanted on the left side, and the NT-Sr implants on the right. The gaps between the implants and extraction sockets were filled with autologous bone chips and X-ray scanning (IntraOs 70, Blue X, Assago, Italy) was performed before teeth extraction, post-extraction, and post-implantation. Antibiotics (ampicillin, 0.5 mg/kg, China) were administered for 5 days to prevent infection post-operation, mouth care with normal saline rinsing was performed for 1 week, and a semi-fluid diet was fed to avoid excessive occlusal force. Twelve weeks after implantation, all animals were euthanized according to the following procedures: overanesthesia with pentobarbital (3%, 100 mg/kg) intravenous injection was applied before harvesting, after vital signs including breathing and heart rate were not detected and tongue cyanosis observed. Mandibles with implants were harvested for subsequent testing. Calcein (8 mg kg⁻¹, Sigma Chemicals Co., United States) and tetracycline (50 mg kg⁻¹, Amresco Ltd., United States) were administered via intramuscular injection on days 4 and 14 to evaluate new bone deposition.

2.3.2 Micro-CT scanning

After euthanasia, the samples were immersed in 75% alcohol and prepared for micro-CT scanning (Inveon, Siemens, Erlangen, Germany). A three-dimensional image was reconstructed using an isotropic voxel size of 15 μm. A region of interest (ROI) was defined as a ring 1 mm in radius from the implant surface. Images acquired from the ROI were used for quantitative analysis, which included bone volume/total volume (BV/TV), trabecular number (Tb.N), trabecular thickness (Tb.Th), and trabecular separation (Tb.Sp).

2.3.3 Histological analysis

The samples were prepared for non-decalcified sections after micro-CT scanning. The samples were immersed in 75% alcohol for 7 days and then dehydrated using a graded series of dilutions of ethanol and 100% acetone. Samples were embedded in polyester resin and cut mid-axially into slices of 150 μm, which were subsequently ground into 100 μm-thick slices using a sawing microtome (Leica SP 1600, Leica Microsystems). Images were captured using a fluorescence microscope (Leica).

After fluorescence observation, the sections were stained with methylene blue acid fuchsin and analyzed using a digitized image analysis system (Leica) coupled to a light microscope (Olympus).

BIC% was calculated as the linear percentage of direct bone-to-implant contact relative to the total implant interface in the cancellous bone.

2.3.4 Biomechanical testing

After the specimens were harvested, eight samples from each group were immediately subjected to a biomechanical pull-out test using a universal material testing system (AGS-10KNG, Shimadzu, Japan). The speed was set at 2 mm/min. The displacement–force curve was recorded to calculate the maximum pull-out force.

2.4 Statistical analysis

Data analysis was performed using the Statistical Package for the Social Sciences (SPSS, version 18). A paired-samples *t*-test was applied for comparisons between two groups. All data are expressed as the mean ± standard deviation (SD). Significant difference was defined as $p < 0.05$, and highly significant differences as $p < 0.01$.

3 Results

3.1 Surface characterization of the samples

SEM images clearly show the surface textures of the two different samples. Nanotubes with diameters of 15–80 nm were distributed on the NT-TiO₂ surface, whereas nanoparticles with diameters of 20–40 nm were deposited on the NT-Sr surface (Figure 1). XPS results showed that Ti, O, and fluorine (F) elements were detected in the NT-TiO₂ samples. The XPS survey of the NT-Sr samples detected the presence of Ti, O, and Sr (Figure 1).

The interface bonding strength of NT-Sr and NT-TiO₂ samples were 52.40 ± 8.73 MPa and 18.20 ± 4.16 MPa, respectively, and a significant difference existed between the groups. SEM images show that the nanotube structure disappeared and that only a residual nanopitted texture remained, whereas the NT-Sr sample displayed a few nanoparticle splits (Figure 1). The contact angles of NT-TiO₂ and NT-Sr were $23.96^\circ \pm 3.64^\circ$ and $29.76^\circ \pm 5.18^\circ$, respectively, which indicated that the NT-TiO₂ surface possessed better hydrophilicity than the NT-Sr surface (Figure 1).

Furthermore, the initial Sr release occurred quickly and the release rate decreased with time. Seven days later, the Sr release rate was relatively constant (Figure 2); the approximate amount of Sr released from NT-Sr samples daily was 0.0156 ± 0.0092 μg/cm². The total Sr content loaded on the NT-Sr surfaces was 42.08 ± 2.52 μg. The results indicated that the total Sr content could be released continuously for over 1 year.

3.2 *In vitro* cellular assay

As shown in Figure 3, the number of adherent cells on all the Ti samples increased from 30 to 120 min, and the number of cells adhered on the NT-TiO₂ surface seemed to be higher than that on the NT-Sr group over the entire process.

Cell proliferation was evaluated using MTT assay (Figure 3). The cells of the two groups proliferated well, with culture times of

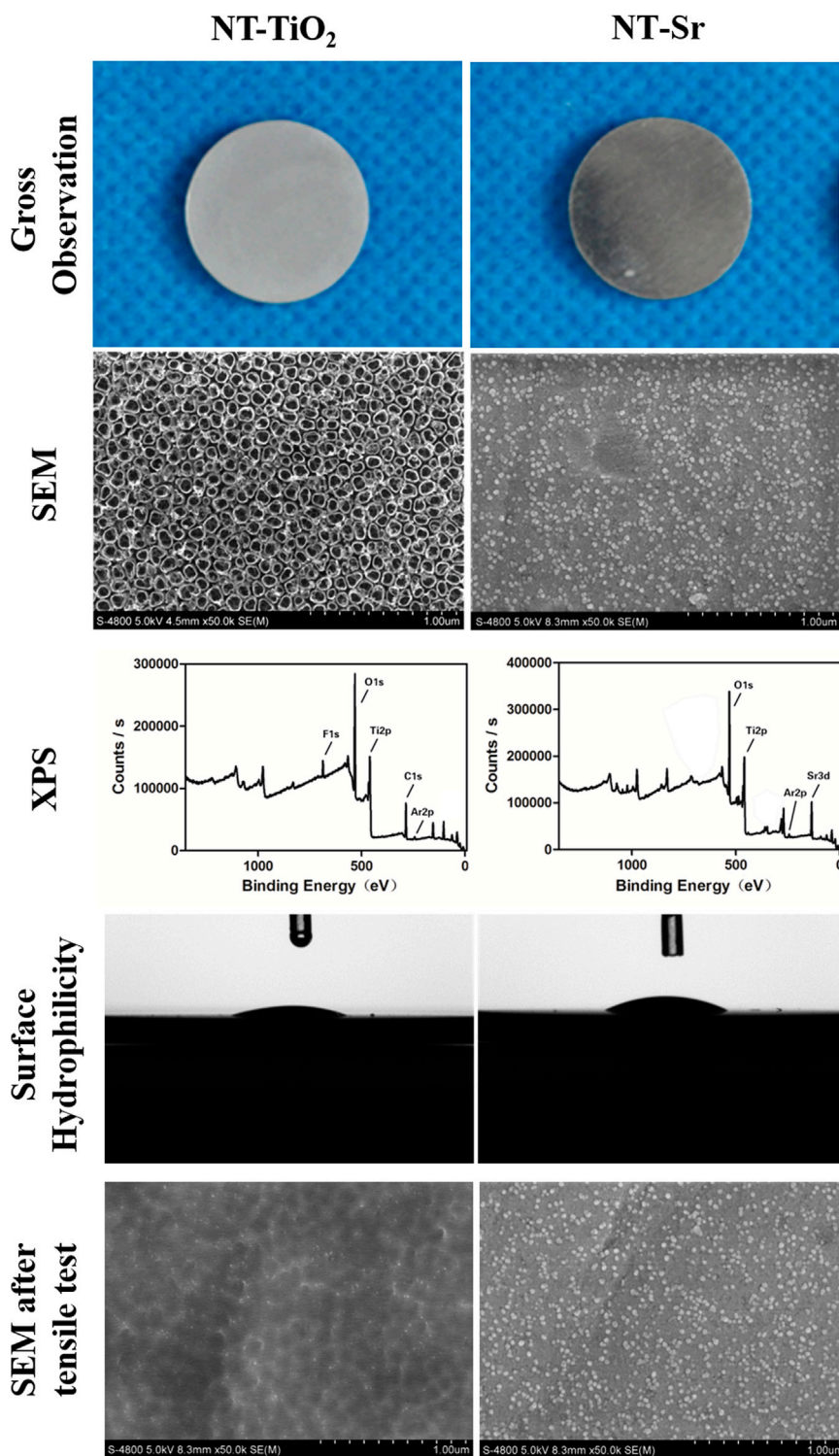


FIGURE 1 Surface characteristics evaluation of the two different samples. ($n = 8$). Scale bar is 200 nm. NT-TiO₂, TiO₂ nanotubes surface; NT-Sr, nano strontium-containing titanium surface; SEM, scanning electron microscopy; XPS, X-ray photoelectron spectroscopy.

1–7 days. On day 1, there was no discernible difference in cell proliferation among the different Ti samples. On days 4 and 7, the NT-TiO₂ samples showed better cell proliferation ability than the NT-Sr samples.

As shown in Figure 3, high-magnification SEM images reveal that osteoblasts had spread on the NT-Sr and NT-TiO₂ surfaces. Compared with the cells grown on NT-Sr, the lamellipodia of the cells grown on NT-TiO₂ spread more smoothly.

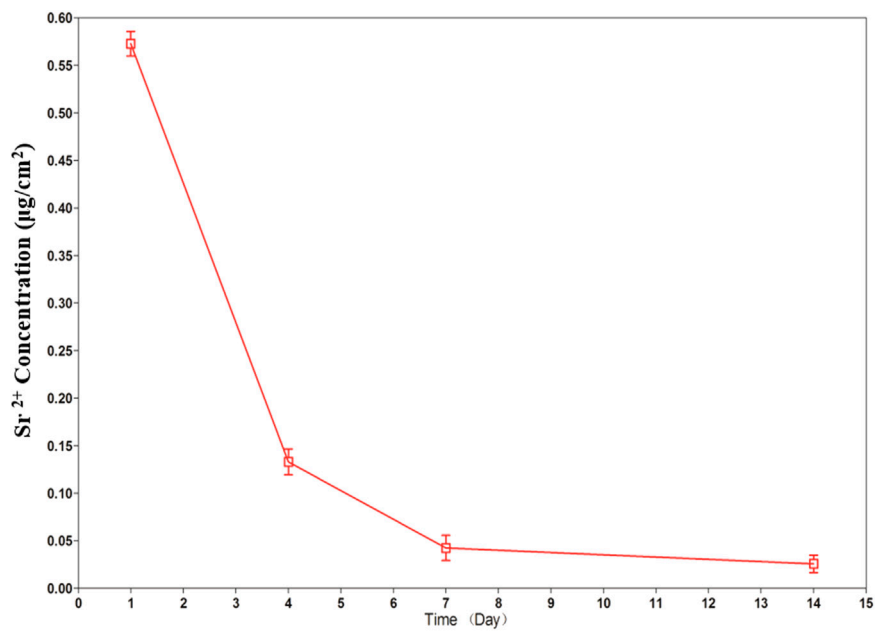


FIGURE 2 Non-cumulative Sr release time profile for NT-Sr into PBS ($n = 5$ at each time point).

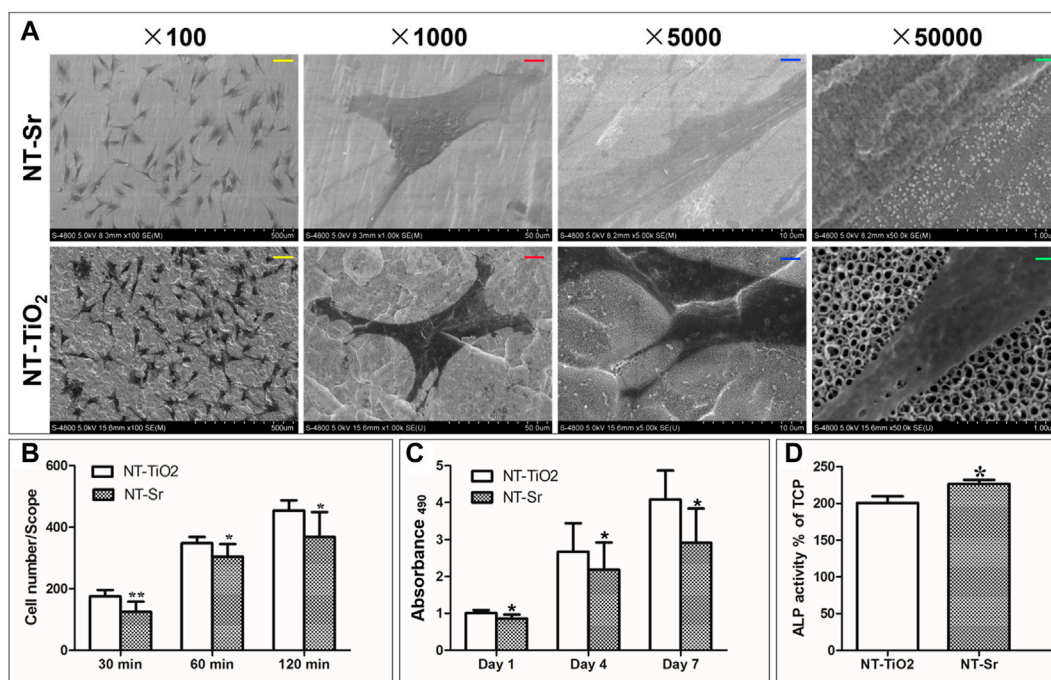


FIGURE 3 *In vitro* cellular activity evaluation of the two different samples. * $p < 0.05$ and ** $p < 0.01$ compared to NT-TiO₂ samples. ($n = 6$ at each time point). (A) SEM images of cellular adhesion on the two surfaces; (B) Cellular attachment on the two different samples; (C) Cellular proliferation after incubation for 1, 4, and 7 days. (D) ALP activity for two samples. Scale bars: yellow scale bar = 100 µm, red scale bar = 10 µm, blue scale bar = 2 µm, green scale bar = 200 nm.

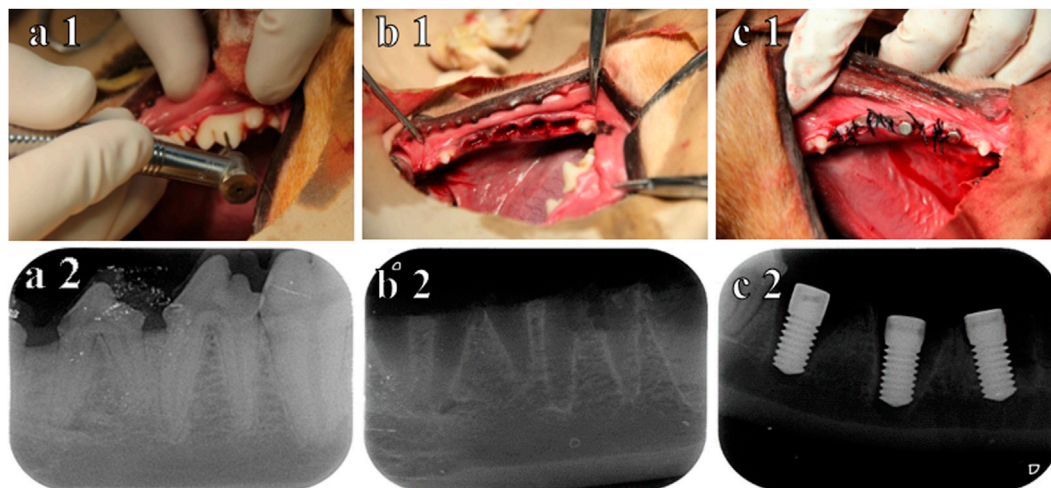


FIGURE 4
 Procedure for immediate implantation and X-ray. **(A1)** before teeth extraction; **(B1)** after teeth extraction; **(C1)** immediately after implantation; **(A2)** X-ray before teeth extraction; **(B2)** X-ray after teeth extraction; **(C2)** X-ray immediately after implantation.

Furthermore, the results in [Figure 3](#) indicate that the NT-Sr group showed significantly better ALP activity after 7 days in culture.

3.3 *In vivo* animal experiment

X-ray examination indicated that the teeth were extracted without additional trauma. Subsequently, the implants were inserted into the extraction socket, and the inferior alveolar neurovascular bundle was not injured ([Figure 4](#)). No implant loss occurred after 3 months of observation.

The 3D reconstructed images from micro-CT are shown in [Figure 5](#), which depict bone remodeling around the implants. The bone volume of the NT-Sr group was higher than that of the NT-TiO₂ group. In the quantitative assessment, BV/TV, Tb.N, and Tb.Th were significantly higher for the NT-Sr group. Particularly, as the most important parameter reflecting bone remodeling, the BV/TV of the NT-Sr group increased 0.91-fold compared to the NT-TiO₂ group ([Table 1](#)).

As shown in the fluorescence microscopy images ([Figure 5](#)), the tissues labelled with calcein were observed with a green fluorescence marker, while those observed with a yellow fluorescence marker indicated tissues labelled with tetracycline; the markers were deposited along the implant surfaces. The mineral apposition ratio (MAR, $\mu\text{m}/\text{d}$) indicates the rate of new-bone mineralization, which is defined as the distance between two double-fluorescence markers. There were statistically significant differences in the MAR between the two groups, in the following order: NT-Sr > NT-TiO₂ ($p < 0.01$). Moreover, from images of the methylene blue/acid fuchsin staining, calcified bone was stained with its characteristic bright pink color and Ti implants were stained black on the slides ([Figure 5](#)). One section from each specimen was used for the analysis, and the results of histomorphometry were expressed

as BIC% ([Table 1](#)). Twelve weeks after implantation, the BIC% of the NT-TiO₂ and NT-Sr groups were $44.13\% \pm 6.2\%$ and $76.63\% \pm 8.16\%$, respectively, and a significant statistical difference in BIC% existed between the two groups.

[Table 2](#) lists the results of the maximal pull-out force of the two groups 12 weeks after implantation. The pull-out force of the NT-Sr group was significantly higher than that of the NT-TiO₂ group ($p < 0.01$).

4 Discussion

Previous clinical and experimental studies have demonstrated that implants immediately inserted in fresh extraction sockets can prevent post-extraction bone loss. However, the immediate implantation strategy has two potential challenges: firstly, gaps between the regular implant and the irregular extraction socket prevent a part of the implant surface from making direct alveolar bone contact ([Naji et al., 2021](#); [Slagter et al., 2021](#)). Secondly, unpredictable implant primary stability results from lower thread mechanical retention in the surrounding bone ([Levin et al., 2021](#)). Therefore, favorable osteogenic ability and primary stability are crucial for immediate implantation success.

Conventionally, the regions where the implant surface directly contacts the host bone facilitate favorable osseointegration, while the regions of mismatch gaps between the implant and extraction socket require better bone induction ability. Compared to micro-topography surfaces, nanotopography appears to positively affect cell behavior, including cell adhesion, spread, motility, and proliferation, and nanotopography can selectively adhere to osteoblasts ([Price et al., 2003](#); [McManus et al., 2005](#)). For example, on nanosized materials, the affinity ratio between osteoblasts and fibroblasts was 3:1, but for conventional materials, the ratio was 1:1 ([Webster et al., 2000](#)).

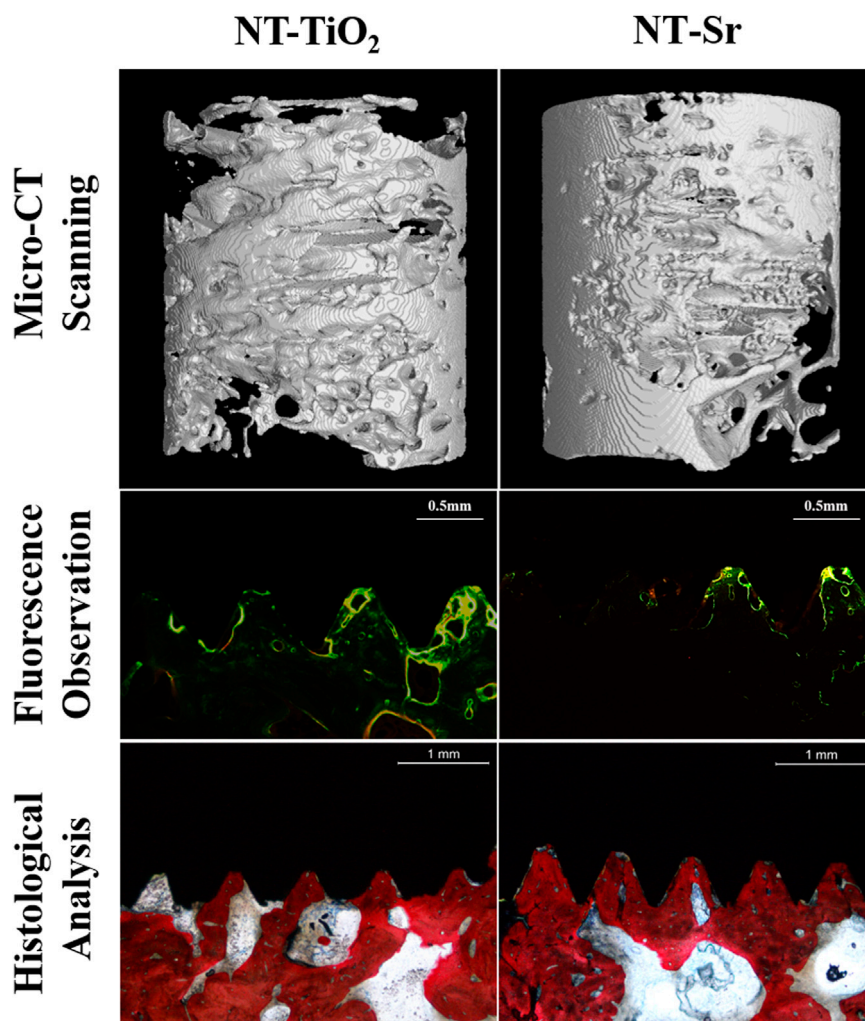


FIGURE 5 Micro-CT scanning ($n = 10$) and histological analysis ($n = 12$) for evaluating osseointegration around the two different surface implants.

TABLE 1 Quantity analysis of trabecular bone from Micro-CT scanning for implantation immediately after teeth extraction * $p < 0.05$ and ** $p < 0.01$ compared with NT-TiO₂ ($n = 10$).

Parameters	Groups	
	NT-TiO ₂	NT-Sr
BV/TV (%)	28.79 ± 5.94	54.95 ± 9.97**
Tb.N (1/mm)	2.06 ± 0.76	2.38 ± 0.46
Tb.Th (μm)	131.6 ± 25.6	204.9 ± 29.7**
Tb.Sp (μm)	315.2 ± 112.7	196.7 ± 89.7*

Nanotopography is crucial for osteogenesis between gaps in the implant surface, which can ensure that osteoblasts, instead of fibroblasts, occupy the gaps between the implant and extraction socket. Therefore, in this study, two typical nanotopographic surfaces, NT-Sr and NT-TiO₂, were applied to promote osteogenesis around titanium implants. SEM imaging indicated

TABLE 2 Histological analysis and biomechanical test for evaluating osseointegration around two different surface implants: * $p < 0.05$ and ** $p < 0.01$ compared with NT-TiO₂ ($n = 12$).

Parameters	Groups	
	NT-TiO ₂	NT-Sr
BIC (%)	44.13 ± 6.2	76.63 ± 8.16**
MAR (μm/day)	1.78 ± 0.55	2.92 ± 0.58**
Maximal pullout force (N)	236.50 ± 40.86	342.75 ± 46.02**

that nanoparticles (20–40 nm) and nanotubes (15–80 nm), respectively, were fabricated on these titanium surfaces. Subsequent *in vitro* cellular assays showed a positive effect on cell adhesion, proliferation, and differentiation. Additionally, compared to the NT-Sr group, the NT-TiO₂ surface showed better cell adhesion and proliferation, which may be attributed to the superior hydrophilicity of the NT-TiO₂ surface. While higher ALP activity was observed on the NT-Sr surface, Sr loading may be

one of the most important factors that influenced bone remodeling. Previous studies have demonstrated that strontium has dual effects on promoting osteogenesis: stimulation of osteoblast differentiation and inhibition of osteoclast functions (Marx et al., 2020). The osseointegration effect of strontium-loaded surfaces under normal and osteoporotic conditions was verified by *in vitro* and *in vivo* experiments (Shi et al., 2017; Liu et al., 2019; López-Valverde, Muriel-Fernández, Gómez de Diego, Ramírez, and; López-Valverde et al., 2019). Moreover, the Sr release assay used in this study detected continuous Sr release at a slow rate, which can ensure active osteogenesis and mineralization. A similar phenomenon was observed in the double fluorescence labelled results, which indicated that the NT-Sr surface possessed a better mineralization ability than the NT-TiO₂ surface.

The animal experiment investigated osseointegration around the implants, and reversed trends from the *in vivo* assay were observed in the two nanotopography groups: the BIC%, MAR, and maximum pull-out strength of the NT-Sr group were higher than those of the NT-TiO₂ group. This can be explained by the results of the epoxy resin docking tensile test, which indicated that the nanocoating interfacial bonding strength of the NT-TiO₂ surface was only 34.73% of that of the NT-Sr surface. SEM imaging after the epoxy resin docking tensile test also showed completely desquamated nanotubes, whereas the NT-Sr surface showed no obvious changes. In clinical practice, a greater range difference is applied to obtain primary stability during immediate implantation; hence, the solid bonding strength between the coating and the titanium substrates is of great importance. Once the coating collapses from the substrates during implant insertion, the free collapsed particles result in potential adverse inflammatory responses, peri-implantitis, and implant loosening. Potential systemic toxicity resulting from desquamate nanoparticles and debris has been reported in previous studies (Hoet et al., 2004; Warheit et al., 2004; Zeman et al., 2018). Therefore, the interfacial bonding strength of the implant and surface coating was comparable to that of the coating and surrounding bones. Considering the above issues, we fabricated a bioactive nanotopography surface using magnetron sputtering technology, which can synthesize highly adherent thin films via physical vapor deposition (PVD) (Stan et al., 2011) (Qadir et al., 2019).

The positive results of the NT-Sr surface in *in vitro* osseointegration satisfied the two main demands of immediate implantation mentioned above. Firstly, nanotopography and Sr loading can promote osteogenesis, which is needed to simultaneously perform implant insertion and tooth extraction. Secondly, a high interfacial bonding strength can resist the strength of a greater insertion force, which is required for better primary stability. Therefore, compared to the NT-TiO₂ surface, the NT-Sr surface is more suitable for immediate implantation.

References

Araújo, M., Silva, C. O., Souza, A. B., and Sukekava, F. (2019). Socket healing with and without immediate implant placement. *Periodontol.* 79,168–177. doi:10.1111/prd.12252

5 Conclusion

Although we tried to take all aspects into consideration, limitations still inevitably existed, such as limited evaluation indicators and a short observation period. Nonetheless, we can conclude from our preliminary results that NT-TiO₂ and NT-Sr surfaces show favorable *in vivo* cellular activity. NT-TiO₂ possessed better cellular adhesion and proliferation due to its higher hydrophilicity. While NT-Sr surfaces with higher coating interfacial bonding strength would be more suitable for immediate implantation, Sr loading on the surface facilitating improved mineralization was another crucial factor.

Data availability statement

The original contributions presented in the study are included in the article/Supplementary material, further inquiries can be directed to the corresponding author.

Ethics statement

The animal study was reviewed and approved by the Laboratory Animal Ethical Inspection, School of the Fourth Military Medical University.

Author contributions

YL: conceptualization, investigation, writing-original draft. LT: investigation, data curation, visualization. MS: investigation, data curation, formal analysis. ZW: investigation, data curation, visualization. XH: conceptualization, revision, writing-review and editing, validation. All authors contributed to the article and approved the submitted version.

Conflict of interest

The authors declare that the research was conducted in the absence of any commercial or financial relationships that could be construed as a potential conflict of interest.

Publisher's note

All claims expressed in this article are solely those of the authors and do not necessarily represent those of their affiliated organizations, or those of the publisher, the editors and the reviewers. Any product that may be evaluated in this article, or claim that may be made by its manufacturer, is not guaranteed or endorsed by the publisher.

Bai, L., Zhao, Y., Chen, P., Zhang, X., Huang, X., Du, Z., et al. (2021). Targeting early healing phase with titania nanotube arrays on tunable diameters to accelerate bone regeneration and osseointegration. *Small* 17, e2006287. doi:10.1002/smll.202006287

- Cavalu, S., Antoniac, I. V., Mohan, A., Bodog, F., Doicin, C., Mates, I., et al. (2020). Nanoparticles and nanostructured surface fabrication for innovative cranial and maxillofacial surgery. *Mater. (Basel)* 13, 5391. doi:10.3390/ma13235391
- Feridoun, P., Javad, Y., Vahid, J., and Solmaz, M. D. (2017). Overview of nanoparticle coating of dental implants for enhanced osseointegration and antimicrobial purposes. *J. Pharm. Pharm. Sci.* 20, 148–160. doi:10.18433/J3GP6G
- Hoet, P. H., Brüske-Hohlfeld, I., and Salata, O. V. (2004). Nanoparticles - known and unknown health risks. *J. Nanobiotechnology*. 2, 12. doi:10.1186/1477-3155-2-12
- Levin, B. P., Chu, S. J., Saito, H., Nevins, M., and Levin, J. P. (2021). A novel implant design for immediate extraction sites: Determining primary stability. *Int. J. Periodontics. Restor. Dent.* 41, 357–364. doi:10.11607/prd.5527
- Li, Y., Qi, Y., Gao, Q., Niu, Q., Shen, M., Fu, Q., et al. (2015). Effects of a micro/nano rough strontium-loaded surface on osseointegration. *Int. J. Nanomedicine*. 10, 4549–4563. doi:10.2147/IJN.S84398
- Liu, F., Li, Y., Liang, J., Sui, W., Bellare, A., and Kong, L. (2019). Effects of micro/nano strontium-loaded surface implants on osseointegration in ovariectomized sheep. *Clin. Implant. Dent. Relat. Res.* 21, 377–385. doi:10.1111/cid.12719
- López-Valverde, N., Muriel-Fernández, J., Gómez de Diego, R., Ramírez, J. M., and López-Valverde, A. (2019). Effect of strontium-coated titanium implants on osseointegration in animal models: A literature systematic review. *Int. J. Oral. Maxillofac. Implants.* 34, 1389–1396. doi:10.11607/jomi.7827
- Marx, D., Rahimnejad Yazdi, A., Papini, M., and Towler, M. (2020). A review of the latest insights into the mechanism of action of strontium in bone. *Bone Rep.* 12, 100273. doi:10.1016/j.bonr.2020.100273
- McManus, A. J., Doremus, R. H., Siegel, R. W., and Bizios, R. (2005). Evaluation of cytocompatibility and bending modulus of nanoceramic/polymer composites. *J. Biomed. Mat. Res. A* 72, 98–106. doi:10.1002/jbm.a.30204
- Mendonça, G., Mendonça, D. B., Aragão, F. J., and Cooper, L. F. (2008). Advancing dental implant surface technology-from micron-to nanotopography. *Biomaterials* 29, 3822–3835. doi:10.1016/j.biomaterials.2008.05.012
- Naji, B. M., Abdelsamea, S. S., Alqutaibi, A. Y., and Said Ahmed, W. M. (2021). Immediate dental implant placement with a horizontal gap more than two millimetres: A randomized clinical trial. *Int. J. Oral. Maxillofac. Surg.* 50, 683–690. doi:10.1016/j.ijom.2020.08.015
- Price, R. L., Gutwein, L. G., Kaledin, L., Tepper, F., and Webster, T. J. (2003). Osteoblast function on nanophase alumina materials: Influence of chemistry, phase, and topography. *J. Biomed. Mat. Res. A* 67, 1284–1293. doi:10.1002/jbm.a.20011
- Qadir, M., Li, Y., and Wen, C. (2019). Ion-substituted calcium phosphate coatings by physical vapor deposition magnetron sputtering for biomedical applications: A review. *Acta. Biomater.* 89, 14–32. doi:10.1016/j.actbio.2019.03.006
- Robo, I., Heta, S., Papakozma, D., and Ostreni, V. (2022). Modification of implant surfaces to stimulate mesenchymal cell activation. *Bull. Natl. Res. Cent.* 46, 52. doi:10.1186/s42269-022-00743-x
- Seyssens, L., Eeckhout, C., and Cosyn, J. (2022). Immediate implant placement with or without socket grafting: A systematic review and meta-analysis. *Clin. Implant. Dent. Relat. Res.* 24, 339–351. doi:10.1111/cid.13079
- Shi, J., Li, Y., Gu, Y., Qiao, S., Zhang, X., and Lai, H. (2017). Effect of titanium implants with strontium incorporation on bone apposition in animal models: A systematic review and meta-analysis. *Sci. Rep.* 7, 15563. doi:10.1038/s41598-017-15488-1
- Slagter, K. W., Meijer, H. J. A., Hentenaar, D. F. M., Vissink, A., and Raghoobar, G. M. (2021). Immediate single-tooth implant placement with simultaneous bone augmentation versus delayed implant placement after alveolar ridge preservation in bony defect sites in the esthetic region: A 5-year randomized controlled trial. *J. Periodontol.* 92, 1738–1748. doi:10.1002/jper.20-0845
- Stan, G. E., Pasuk, I., Husanu, M. A., Enculescu, I., Pina, S., Lemos, A. F., et al. (2011). Highly adherent bioactive glass thin films synthesized by magnetron sputtering at low temperature. *J. Mat. Sci. Mat. Med.* 22, 2693–2710. doi:10.1007/s10856-011-4441-1
- Warheit, D. B., Laurence, B. R., Reed, K. L., Roach, D. H., Reynolds, G. A., and Webb, T. R. (2004). Comparative pulmonary toxicity assessment of single-wall carbon nanotubes in rats. *Toxicol. Sci.* 77, 117–125. doi:10.1093/toxsci/kfg228
- Webster, T. J., Ergun, C., Doremus, R. H., Siegel, R. W., and Bizios, R. (2000). Specific proteins mediate enhanced osteoblast adhesion on nanophase ceramics. *J. Biomed. Mat. Res.* 51, 475–483. doi:10.1002/1097-4636(20000905)51:3<475:aid-jbm23>3.0.co;2-9
- Yeo, I. (2019). Modifications of dental implant surfaces at the micro- and nano-level for enhanced osseointegration. *Materials* 13, 89. doi:10.3390/ma13010089
- Zeman, T., Loh, E. W., Čierný, D., and Šerý, O. (2018). Penetration, distribution and brain toxicity of titanium nanoparticles in rodents' body: A review. *IET. Nanobiotechnol.* 12, 695–700. doi:10.1049/iet-nbt.2017.0109